Journal of Fluid Mechanics
http://journals.cambridge.org/FLM

Additional services for ***Journal of Fluid Mechanics:***

Email alerts: Click here
Subscriptions: Click here
Commercial reprints: Click here
Terms of use : Click here

Hypersonic aerodynamics on thin bodies with interaction and upstream influence

A. Farid Khorrami and Frank T. Smith

Journal of Fluid Mechanics / Volume 277 / October 1994, pp 85 - 108
DOI: 10.1017/S0022112094002697, Published online: 26 April 2006

Link to this article: http://journals.cambridge.org/abstract_S0022112094002697

How to cite this article:
A. Farid Khorrami and Frank T. Smith (1994). Hypersonic aerodynamics on thin bodies with interaction and upstream influence. Journal of Fluid Mechanics, 277, pp 85-108 doi:10.1017/S0022112094002697

Request Permissions : Click here

CAMBRIDGE JOURNALS

Downloaded from http://journals.cambridge.org/FLM, IP address: 144.82.107.36 on 18 Oct 2012

J. Fluid Mech. (1994), *vol.* 277, *pp.* 85–108

Copyright © 1994 Cambridge University Press

Hypersonic aerodynamics on thin bodies with interaction and upstream influence

By A. FARID KHORRAMI[1]† AND FRANK T. SMITH[2]

[1] Department of Engineering Science, Oxford University, Parks Road, Oxford, OX1 3PJ, UK

[2] Department of Mathematics, University College London, Gower Street, London WC1E 6BT, UK

(Received 28 November 1992 and in revised form 5 May 1994)

In the fundamental configuration studied here, a steady hypersonic free stream flows over a thin sharp aligned airfoil or flat plate with a leading-edge shock wave, and the flow field in the shock layer (containing a viscous and an inviscid layer) is steady laminar and two-dimensional, for a perfect gas without real and high-temperature gas effects. The viscous and inviscid layers are analysed and computed simultaneously in the region from the leading edge to the trailing edge, including the upstream-influence effect present, to determine the interactive flow throughout the shock layer and the positions of the shock wave and the boundary-layer edge, where matching is required. Further theoretical analysis of the shock layer helps to explain the computational results, including the nonlinear breakdown possible when forward marching against enhanced upstream influence, for example as the wall enthalpy increases towards its insulated value. Then the viscous layer is computed by sweeping methods, for higher values of wall enthalpies, to prevent this nonlinear breakdown for airfoils including the flat plate. Thin airfoils in hypersonic viscous flow are treated, for higher values of the wall enthalpies and with the upstream-influence effect, as are hypersonic inviscid flows, by modifying the computational methods used for the flat plate. Also, the behaviour of the upstream influence for bodies of relatively large thickness, and under wall velocity slip and enthalpy jump for flat plates, is discussed briefly from a theoretical point of view.

Subsequent to the present work, computations based on the Navier–Stokes and on the parabolized Navier–Stokes equations have yielded excellent and good agreement respectively with the present predictions for large Mach and Reynolds numbers.

1. Introduction

When a continuum hypersonic free stream flows over a sharp airfoil or flat plate with an attached leading-edge shock wave, the hypersonic shock layer, that is the flow field from the leading edge to the trailing edge and from the wall to the shock wave, consists of different regions as follows. In the lateral direction the shock layer contains a viscous and inviscid layer, which are governed by the Prandtl boundary layer and a form of the Euler equations of motion, and here are referred as VL and IL respectively. Lees & Probstein (1952) have shown that the existence of the inviscid layer, with a relatively cool high-density and large gas flux, between the shock wave and the outer edge of the viscous layer, with a very high temperature and low density and gas flux, is necessary

† Present address: Department of Mathematics, University College London, Gower Street, London WC1E 6BT, UK.

as this outer edge must be a streamline which cannot coincide with the shock wave. The basic flow structure involved here has been addressed by numerous authors, for example see Hayes & Probstein (1959) or Stewartson (1964). Very close to the leading edge of the thin airfoil or plate a small kinetic region exists, which is non-continuum and of the order of a few mean free paths downstream of the leading-edge tip. This is followed by the merged region, where the viscous boundary layer and the shock wave are indistinguishable; the shock wave is not fully developed yet and its structure is relatively thick. The streamwise length of the merged region increases appreciably as the Mach number and/or the inverse of the Reynolds number increase. At hypersonic speeds over slender bodies, the shock wave lies so close to the body surface that the boundary layer must exert a strong influence on the flow field. Furthermore, downstream of the merged region, the flow inside the inviscid layer is affected due to the rapid growth of the boundary layer near the leading edge, deflecting the incoming streamlines upward, which in turn feeds back into the viscous layer, affecting its properties and the growth of the boundary layer and resulting in a mutual viscous interaction between the two layers. So the merged layer downstream asymptotically approaches a strong, followed by a moderate and finally a weak interaction region, dominated by the pressure interaction, which is a consequence of viscous interaction. The process is governed by the hypersonic viscous interaction parameter known as χ, which is respectively much larger than unity, of order unity, and much smaller than unity in the above interaction regions. In the interaction regions the shock wave is fully developed and can be treated as a discontinuity, using the Rankine–Hugoniot shock relationships.

The flow configuration based essentially on the flat-plate case is clearly one of the most fundamental in hypersonic aerodynamics. Moreover, it allows a gradual build-up to be made towards cases of thicker bodies which are of more practical application, and it also encompasses a range of surface conditions including in particular low wall enthalpies which again are more realistic. The build-up just mentioned and the surface conditions are discussed later. Concerning the underlying, interactive, flow structure in the hypersonic boundary layer motion it is known that the appropriately scaled gas temperature vanishes at the outer edge of the boundary layer and the same happens with the viscosity. Therefore, the position of this edge can be determined precisely, in contrast with that for a boundary layer at lower Mach number. At first order the boundary layer has a sharply defined edge which acts as a streamline, when the free-stream Mach number tends to infinity, causing the temperature to become large and consequently the density to become small inside the boundary layer; thus the boundary layer tends to resemble a vacuum. Also at first order, the streamwise and transverse velocities and the pressure are continuous as the boundary-layer edge is approached, but the temperature and the density change in order-of-magnitude terms on passing from the viscous to the inviscid layer. The streamwise velocity also does not match directly between the viscous and inviscid layers, at second order. However, these apparent mismatches are resolved in an infinitesimally narrow region, the so-called vorticity layer, present at the boundary-layer edge, which as mentioned above tends to become a streamline as the free-stream Mach number approaches infinity. The sharp edge is really a narrow asymptotic transitional layer between the outer and inner edges of the viscous and inviscid layers, mainly for higher-order approximations. Studies of this transitional layer are based on the fact that the first-order boundary-layer temperature decays exponentially while the second-order decay is algebraic; so the leading boundary-layer approximation must fail, from the asymptotic point of view, somewhere near the outer edge, and possibly also in all higher-order approximations,

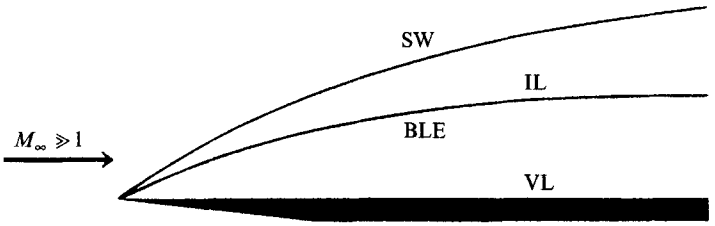

FIGURE 1. The flow structure of a thin sharp body such as the flat plate in a hypersonic free stream, investigated here. SW and BLE indicate the shock wave and the boundary-layer edge, and IL and VL the inviscid and viscous layers.

see for example Lee & Cheng (1969). In addition, for a sharp flat plate the entropy gradient is small since the shock is not as highly curved around the leading edge as for a blunt body. Indeed, the entropy layer is thinner than the viscous layer in this case and its effect can be ignored. Furthermore, for slender bodies high-temperature gas effects may be taken to be insignificant.

It is perhaps surprising that the fundamental flow problem of concern here has not been solved fully. The reason is almost certainly that a somewhat detailed treatment is required that combines analysis and rather large-scale computations to achieve accuracy. This is the aim of the present work. By comparison direct numerical simulations of the Navier–Stokes equations tend to struggle for accuracy in the range of Mach numbers and Reynolds numbers of practical concern here, approximately a free-stream Mach number of 10 and a Reynolds number of 10^8 say. In similar vein, accurate solutions for the steady basic flows are needed for use in subsequent stability and transition analyses; see for example Brown *et al.* (1991). One notes for instance the importance of the vorticity layer with regard to the dominant inviscid mode of instability in the hypersonic boundary layer (Smith & Brown 1990), in addition to the subdominant inviscid modes (Smith & Brown 1990; Cowley & Hall 1990) which depend on the entire viscous-layer properties. Non-parallel-flow effects also become significant for the viscous modes at large free-stream Mach numbers (Smith 1989).

In the following, the first-order non-dimensional equations of motion are derived in §2 along with their boundary conditions. The hypersonic shock layer over the entire body is computed using finite-difference methods, as discussed in §§3–5, and also see figure 1. Furthermore, comparisons with computations based on the Navier–Stokes and on the parabolized Navier–Stokes equations (J. J. Korte 1993, personal communication) are provided in §3. Particular attention is given in §5 to the major feature of upstream influence, which can cause a nonlinear breakdown of the solutions if numerical marching is used purely in the downstream direction, and discussions are also presented on the effects of the hypersonic interaction parameter, the wall enthalpy, possible wall velocity slip, and increasing body thickness, from an analytical point of view to explain the computational results. In response to referees' comments, a point of note concerns the flow behaviour near the trailing edge. There, if the flow is subsonic or supersonic there is a local triple-deck structure to account for the abrupt change in the boundary conditions: see Stewartson (1968, 1969), Messiter (1970), Jobe & Burggraf (1974), Smith (1983) among others. However, as the Mach number increases, the interactive triple-deck structure elongates in the streamwise direction and in fact the interaction length becomes comparable with the airfoil length exactly as the regime of current interest is entered, i.e. as the Mach number becomes $O(Re^{1/6})$, so that the hypersonic interaction parameter becomes $O(1)$. So in effect there is then no triple-deck at the trailing edge. The above was shown by Neiland (1970) and Brown & Stewartson

(1975). The same lengthening is associated with upstream influence since the latter is also controlled by the triple-deck structure at lower Mach numbers. Along with this, at the onset of the trailing edge the non-vanishing of the wall shear stress, which is a feature common to the trailing-edge interactions above at lower Mach numbers, naturally remains a feature of the present long-scale interaction. The computational methods described in §5 are developed to compute the hypersonic viscous flow over thin bodies and bring in directly the effect of upstream influence. These methods are used to compute the flow fields over thin airfoils in viscous–inviscid or purely inviscid hypersonic flows as presented in §6. Finally, in §7, further comments are made and the overall results are discussed and compared.

2. The equations of motion

The viscous layer is governed by the Prandtl boundary-layer equations, as shown for example by Shen (1952), Lees (1953) and Khorrami (1991). So the equations of continuity, streamwise momentum and energy are

$$\frac{\partial(\rho^* u^*)}{\partial x^*}+\frac{\partial(\rho^* v^*)}{\partial y^*}=0, \tag{2.1}$$

$$\rho^* u^*\frac{\partial u^*}{\partial x^*}+\rho^* v^*\frac{\partial u^*}{\partial y^*}=-\frac{\partial p^*}{\partial x^*}+\frac{\partial}{\partial y^*}\left(\mu^*\frac{\partial u^*}{\partial y^*}\right), \tag{2.2}$$

$$\rho^* u^*\frac{\partial H^*}{\partial x^*}+\rho^* v^*\frac{\partial H^*}{\partial y^*}=\frac{\partial}{\partial y^*}\left(\frac{\mu^*}{Pr}\frac{\partial H^*}{\partial y^*}\right)+\frac{\partial}{\partial y^*}\left[\left(1-\frac{1}{Pr}\right)\mu^* u^*\frac{\partial u^*}{\partial y^*}\right], \tag{2.3}$$

respectively, where Pr is the Prandtl number, and * refers to the dimensional physical quantities such as the streamwise and transverse velocities u^* and v^*, density ρ^*, viscosity μ^*, total enthalpy H^*, streamwise and transverse distances x^* and y^*. The equation of transverse momentum is $\partial p^*/\partial y^* = 0$, which implies that the pressure is constant across the viscous layer. The inviscid layer is described by a form of the compressible Euler equations of motion, the equations of streamwise and transverse momentum and energy being

$$\rho^* u^*\frac{\partial u^*}{\partial x^*}+\rho^* v^*\frac{\partial u^*}{\partial y^*}=-\frac{\partial p^*}{\partial x^*}, \tag{2.4}$$

$$\rho^* u^*\frac{\partial v^*}{\partial x^*}+\rho^* v^*\frac{\partial v^*}{\partial y^*}=-\frac{\partial p^*}{\partial y^*}, \tag{2.5}$$

$$\rho^* u^*\frac{\partial p^*}{\partial x^*}+\rho^* v^*\frac{\partial p^*}{\partial y^*}=\gamma p^*\left(u^*\frac{\partial \rho^*}{\partial x^*}+v^*\frac{\partial \rho^*}{\partial y^*}\right), \tag{2.6}$$

respectively. The equation of continuity is the same as above. The equations of state throughout the shock layer assuming a perfect gas with a ratio γ of specific heats equal to 1.4 for air, of stagnation enthalpy in the viscous layer, and of the linear temperature-viscosity law, are

$$p^* = \rho^* R^* T^*, \tag{2.7}$$

$$H^* = \frac{\gamma}{\gamma-1}\frac{p^*}{\rho^*}+\frac{u^{*2}+v^{*2}}{2}, \tag{2.8}$$

$$\mu^*/\mu^*_\infty = C\,T^*/T^*_\infty. \tag{2.9}$$

Here R^*, C being nearly unity (here taken to be unity), are the universal gas and Chapman–Rubesin constants respectively. The hypersonic interaction parameter used here, somewhat different from the classical $M_\infty^3(C/Re_\infty)^{1/2}$, and the small perturbation parameter, are defined as

$$\chi = \frac{M_\infty}{Re_\infty^{1/6}} \geqslant O(1), \quad \epsilon = \frac{M_\infty^{1/2}}{Re_\infty^{1/4}} = \frac{\chi^{3/2}}{M_\infty} \ll 1. \tag{2.10}$$

The Reynolds number is $Re_\infty = \rho_\infty^* U_\infty^* L^*/\mu_\infty^*$, where L^* is the thin-airfoil chord or the flat-plate length, and the subscript ∞ refers to the free-stream conditions.

The flow variables are expanded next in terms of powers of the small perturbation parameter and the free-stream Mach number, in accordance with the theory of hypersonic boundary-layer interaction and small perturbations for inviscid flow, as follows (Stewartson 1964; Neiland 1970; Brown & Stewartson 1975). The non-dimensional asymptotic representations, given that the pressure in the viscous layer and the boundary-layer edge δ^* are streamwise dependent only, have the form

$$\left(\frac{x^*}{L^*}\ \frac{y^*}{L^*}\ \frac{\delta^*}{L^*}\ \frac{u^*}{U_\infty^*}\ \frac{v^*}{U_\infty^*}\ \frac{p^*}{p_\infty^*}\ \frac{\rho^*}{\rho_\infty^*}\ \frac{\mu^*}{\mu_\infty^*}\ \frac{T^*}{T_\infty^*}\ \frac{H^*}{U_\infty^{*2}}\right)^T$$

$$\left.\begin{aligned}&(x\ \epsilon y\ \epsilon\delta\ u\ \epsilon v\ \epsilon^2\gamma M_\infty^2 p\ \epsilon^2\rho\ M_\infty^2\mu\ \gamma M_\infty^2 T\ H)^T + \ldots \text{ in VL},\\ &(x\ \epsilon y\ \epsilon\delta\ 1+\epsilon^2 u\ \epsilon v\ \epsilon^2\gamma M_\infty^2 p\ \rho\ 0\ \epsilon^2\gamma M_\infty^2 T\ \tfrac{1}{2}+\epsilon^2 H)^T + \ldots \text{ in IL.}\end{aligned}\right\} \tag{2.11}$$

These are substituted into the Prandtl boundary-layer equations and after collection of the dominant terms the asymptotic equations of continuity, streamwise momentum, energy, state, total enthalpy and linear temperature–viscosity law, from (2.1)–(2.3), (2.7)–(2.9), are respectively

$$\frac{\partial(\rho u)}{\partial x} + \frac{\partial(\rho v)}{\partial y} = 0, \tag{2.12}$$

$$\rho u\frac{\partial u}{\partial x} + \rho v\frac{\partial u}{\partial y} = -\frac{\partial p}{\partial x} + \frac{\partial}{\partial y}\left(\mu\frac{\partial u}{\partial y}\right), \tag{2.13}$$

$$\rho u\frac{\partial H}{\partial x} + \rho v\frac{\partial H}{\partial y} = \frac{\partial}{\partial y}\left(\frac{\mu}{Pr}\frac{\partial H}{\partial y}\right) + \frac{\partial}{\partial y}\left[\left(1-\frac{1}{Pr}\right)\mu u\frac{\partial u}{\partial y}\right], \tag{2.14}$$

$$p = \rho T, \tag{2.15}$$

$$H = \tfrac{1}{2}u^2 + \frac{\gamma}{\gamma-1}\frac{p}{\rho}, \tag{2.16}$$

$$\mu = \gamma C T. \tag{2.17}$$

The transverse pressure stays constant even to second order. The same results can be obtained by substitution into the Navier–Stokes equations in the double limit of the Mach number and the Reynolds number approaching infinity.

Similarly, from substituting the above expansions into the Euler equations (2.1), (2.4)–(2.6), and following a similar procedure, the first-order equations of continuity, streamwise and transverse momentum and energy in the inviscid layer are

$$\frac{\partial\rho}{\partial x} + \frac{\partial(\rho v)}{\partial y} = 0, \tag{2.18}$$

$$\rho\frac{\partial u}{\partial x}+\rho v\frac{\partial u}{\partial y}=-\frac{\partial p}{\partial x}, \tag{2.19}$$

$$\rho\frac{\partial v}{\partial x}+\rho v\frac{\partial v}{\partial y}=-\frac{\partial p}{\partial y}, \tag{2.20}$$

$$\rho\frac{\partial p}{\partial x}+\rho v\frac{\partial p}{\partial y}=\gamma p\left(\frac{\partial \rho}{\partial x}+v\frac{\partial \rho}{\partial y}\right), \tag{2.21}$$

respectively. The equation of enthalpy is $H=u+\frac{1}{2}v^2+\gamma p/(\gamma-1)\rho$ but the equation of state remains the same as in the viscous layer.

It is assumed that the wall is insulated or it has a constant enthalpy with no velocity slip. At the boundary-layer edge the streamwise velocity is to be approximately the same as the free-stream velocity, while the transverse velocity is proportional to the scaled rate of growth of the boundary-layer displacement thickness, which is large near the leading edge and smaller further downstream. Therefore the boundary conditions at the wall and at the boundary-layer edge are respectively

$$u=v=0, \quad \frac{\partial H}{\partial y}=0 \quad \text{or} \quad H=H_w, \tag{2.22}$$

and

$$u=1, \quad v=\frac{\mathrm{d}\delta}{\mathrm{d}x}, \quad H=\tfrac{1}{2}, \tag{2.23}$$

where subscript w indicates the wall conditions.

Assuming that the unknown shock shape is described by $y^*=\epsilon x^* g(x)$, it can be shown that its slope $\mathrm{d}y^*/\mathrm{d}x^*$ is of order M_∞^{-1}, since in hypersonic flow the shock wave lies very close to the body, resulting in a small shock angle. Then from the Rankine–Hugoniot shock relationships the boundary conditions at the shock wave are:

$$\left.\begin{aligned} u_s&=-\frac{2}{\gamma+1}\left(\frac{\mathrm{d}g}{\mathrm{d}x}\right)^2(1-\chi_1), & v_s&=\frac{2}{\gamma+1}\frac{\mathrm{d}g}{\mathrm{d}x}(1-\chi_1),\\ p_s&=\frac{2}{\gamma+1}\left(\frac{\mathrm{d}g}{\mathrm{d}x}\right)^2\left(1-\frac{\gamma-1}{2\gamma}\chi_1\right), & \rho_s&=\frac{\gamma+1}{\gamma-1}\left(1+\frac{2\chi_1}{\gamma-1}\right)^{-1}, \end{aligned}\right\} \tag{2.24}$$

for the velocities, pressure and density respectively, where the subscript s indicates the shock conditions and $\chi^{3/2}(\mathrm{d}g/\mathrm{d}x)=\chi_1^{-1/2}$. Also the orders of magnitude of the flow variables at the shock wave, $u_s^*/U_\infty^*\sim 1+O(M_\infty^{-2})$, $v_s^*/U_\infty^*=O(M_\infty^{-1})$, $p_s^*/p_\infty^*=O(1)$, $\rho_s^*/\rho_\infty^*=O(1)$, are in keeping with the representations in the inviscid layer in (2.11). In general, for example for airfoil shapes and finite-length bodies, the values of the hypersonic interaction parameter and consequently of the Mach number, via the shock-wave equations, affect the solution of the inviscid layer, and in turn of the viscous layer, since the solutions of these two layers interact. On the other hand, for a semi-infinite plate the first-order representations can be chosen such that the orders of magnitude, the equations of motion and the boundary conditions remain the same but the interaction parameter is replaced by unity in the shock-wave conditions (2.24), and the dimensional streamwise distance is now $x^*\propto\chi^6$. Hence, for the special case of a semi-infinite plate (see also figure 4 below), the interactive flow is in effect independent of the interaction parameter and the free-stream Mach number. In addition it is noted that in higher-order approximations the choice of a linear or

nonlinear temperature–viscosity law is important during the matching of the solution, since the latter gives a higher-order magnitude of gas flux in the transitional layer compared with the boundary layer itself.

Finally it is observed that in hypersonic flow a classical way of predicting the body-surface pressure is to use the tangent-wedge approximation (see for example Hayes & Probstein 1959) for two-dimensional and moderately slender bodies. The pressure at first order, using the tangent-wedge approximation and the scalings of (2.11) can then be expressed as

$$p = \frac{1}{\gamma\chi^3} + \frac{\gamma+1}{4}\left(\frac{\mathrm{d}\delta}{\mathrm{d}x}\right)^2 + \frac{\mathrm{d}\delta}{\mathrm{d}x}\left[\left(\frac{\gamma+1}{4}\frac{\mathrm{d}\delta}{\mathrm{d}x}\right)^2 + \frac{1}{\chi^3}\right]^{1/2}, \tag{2.25}$$

which is used later (see §§4 and 5). Although this approximation gives no information about the structure of the inviscid layer, it is sometimes a helpful alternative to solving (2.18)–(2.21) with (2.23), (2.24) and, as seen later, it works well in comparison.

3. Hypersonic shock layer over an entire body

The complete hypersonic shock layer is treated numerically here, to determine the flow variables in the viscous and inviscid layers and the positions of the boundary-layer edge and the shock wave. The coordinates x, y in the viscous and inviscid layers are transformed to ξ, η such that

$$\xi = x, \quad 0 \leqslant \xi \leqslant 1 \quad \text{and} \quad \eta = \frac{y}{\delta} \text{ in VL} \quad \text{or} \quad \frac{y-\delta}{g-\delta} \text{ in IL}, \quad 0 \leqslant \eta \leqslant 1. \tag{3.1}$$

This transforms the smooth curves of the boundary-layer edge and the shock wave to straight lines at $\eta = 1$, as in figure 2. Then in this coordinate system, from (2.12)–(2.14), the viscous-layer equations of continuity, streamwise momentum and energy become

$$\frac{\partial(\rho u)}{\partial\xi} - \frac{\eta}{\delta}\frac{\mathrm{d}\delta}{\mathrm{d}\xi}\frac{\partial(\rho u)}{\partial\eta} + \frac{1}{\delta}\frac{\partial(\rho v)}{\partial\eta} = 0, \tag{3.2}$$

$$\rho u\left(\frac{\partial u}{\partial\xi} - \frac{\eta}{\delta}\frac{\mathrm{d}\delta}{\mathrm{d}\xi}\frac{\partial u}{\partial\eta}\right) + \frac{\rho v}{\delta}\frac{\partial u}{\partial\eta} = -\frac{\partial p}{\partial\xi} + \frac{1}{\delta^2}\frac{\partial}{\partial\eta}\left(\mu\frac{\partial u}{\partial\eta}\right), \tag{3.3}$$

$$\rho u\left(\frac{\partial H}{\partial\xi} - \frac{\eta}{\delta}\frac{\mathrm{d}\delta}{\mathrm{d}\xi}\frac{\partial H}{\partial\eta}\right) + \frac{\rho v}{\delta}\frac{\partial H}{\partial\eta} = \frac{1}{\delta^2}\frac{\partial}{\partial\eta}\left[\frac{\mu}{Pr}\frac{\partial H}{\partial\eta} + \left(1 - \frac{1}{Pr}\right)\mu u\frac{\partial u}{\partial\eta}\right], \tag{3.4}$$

respectively, and similarly the inviscid-layer equations of continuity, transverse momentum and energy become

$$f_1\frac{\partial\rho}{\partial\xi} + f_2\frac{\partial\rho}{\partial\eta} + \rho\frac{\partial v}{\partial\eta} = 0, \tag{3.5}$$

$$\rho f_1\frac{\partial v}{\partial\xi} + \rho f_2\frac{\partial v}{\partial\eta} + \frac{\partial p}{\partial\eta} = 0, \tag{3.6}$$

$$f_1\left(\rho\frac{\partial p}{\partial\xi} - \gamma p\frac{\partial\rho}{\partial\xi}\right) + f_2\left(\rho\frac{\partial p}{\partial\eta} - \gamma p\frac{\partial\rho}{\partial\eta}\right) = 0, \tag{3.7}$$

respectively from (2.18)–(2.21). Here $f_1 = g - \delta$ and $f_2 = (\eta - 1)(\mathrm{d}\delta/\mathrm{d}\xi) - \eta(\mathrm{d}g/\mathrm{d}\xi) + v$. In the inviscid layer the streamwise velocity is effectively redundant.

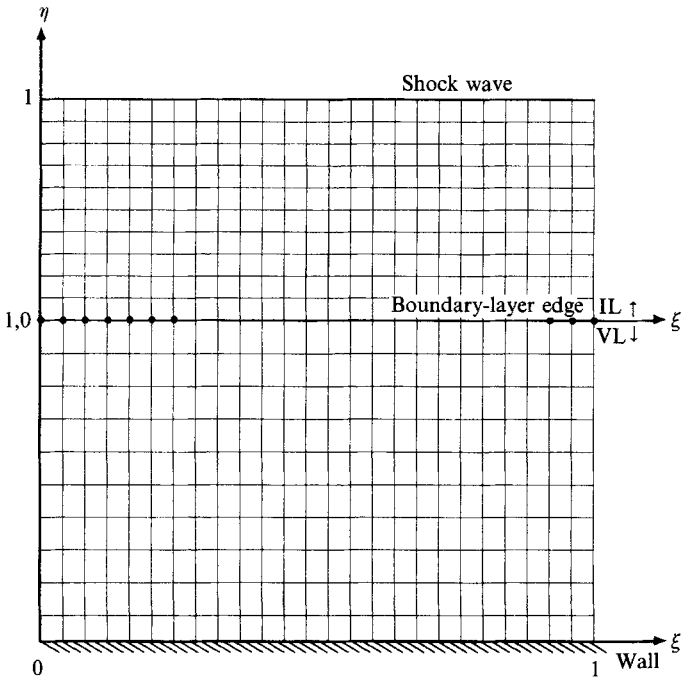

FIGURE 2. The hypersonic shock layer, i.e. the domain of computation in the transformed coordinates. The boundary-layer edge is at η of unity and zero in the VL and IL respectively.

The flow variables in the viscous and inviscid layers depend on the streamwise and transverse coordinates in general, whereas the positions of the boundary-layer edge and the shock wave are dependent on the streamwise distance only. Near the leading edge as the streamwise distance approaches zero, that is in the strong interaction region associated with high values of the interaction parameter, these quantities acquire a similarity form. It can be shown that in terms of the streamwise dependence, the flow variables in the viscous layer behave as $v \sim x^{-1/4}$, $p \sim x^{-1/2}$, $\rho \sim x^{-1/2}$, $\delta \sim x^{3/4}$ with u, T, H and μ being of the order of unity, and in the inviscid layer $u \sim x^{-1/2}$, $v \sim x^{-1/4}$, $p \sim x^{-1/2}$, $\rho \sim O(1)$, $T \sim x^{-1/2}$, $H \sim x^{-1/2}$ and $g \sim x^{3/4}$. This behaviour of the flow variables provides the basis for determining the similarity solution near the leading edge. The existence of the similarity solution in either layer has been established for the flat plate (for example see Stewartson 1955; 1964, chapter 7, part II), and here the computations are, in what follows, for the flat plate and airfoil. This leading-edge behaviour stays intact for airfoil shapes that are of order $x^{3/4}$ or less in thickness.

Following the streamwise behaviour of the flow variables near the leading edge, then downstream, in the viscous layer these variables are written

$$\left.\begin{aligned} &u = \bar{u}, \quad v = C_2 \xi^{-1/4} \bar{v}, \quad p = C_1 \xi^{-1/2} \bar{p}, \quad \rho = C C_2^{-2} \xi^{-1/2} \bar{\rho}, \\ &T = \bar{T}, \quad H = \bar{H}, \quad \mu = C\bar{\mu}, \quad \delta = C_2 \xi^{3/4} \bar{\delta}, \end{aligned}\right\} \tag{3.8}$$

and in the inviscid layer

$$\left.\begin{aligned} &u = C_2^2 \xi^{-1/2} \bar{u}, \quad v = C_2 \xi^{-1/4} \bar{v}, \quad p = C_2^2 \xi^{-1/2} \bar{p}, \quad \rho = \bar{\rho}, \\ &T = C_2^2 \xi^{-1/2} \bar{T}, \quad H = C_2^2 \xi^{-1/2} \bar{H}, \quad \delta = C_2 \xi^{3/4} \bar{\delta}, \quad g = C_4 \xi^{3/4} \bar{g}. \end{aligned}\right\} \tag{3.9}$$

Here $C_1 = CC_3/C_2^2$, C_2, C_3 and $C_4 = C_2 C_5$ are unknown constants. All functions on the right-hand sides of (3.8), (3.9) referred to as $\bar{f}$ are different in each layer, except for $\bar{\delta}$, and are dependent on ξ, η except for $\bar{p}$ in the viscous layer, and $\bar{\delta}$, $\bar{g}$ which are streamwise dependent only. Moreover, to avoid the irregularities at the boundary-layer edge, the transverse coordinate η is stretched to ζ such that

$$\zeta = \int_0^1 \bar{\rho}(\xi, \eta)\, \mathrm{d}\eta/(\gamma C_3)^{1/2},$$

where ζ approaches infinity near the leading edge since it is approximately $[-\ln(1-\eta)]^{1/2}$ there. The stream function $\psi(\xi, \eta)$ is chosen as

$$\tfrac{1}{4}\psi + \xi\psi_\xi = \bar{\rho}(\bar{f}_1 + \xi\eta\bar{u}\bar{\delta}_\xi)/(\gamma C_3)^{1/2}, \quad \psi_\eta = \bar{u}\bar{\rho}\bar{\delta}/(\gamma C_3)^{1/2}, \tag{3.10}$$

to satisfy the continuity equation, and the differentiation is with respect to the subscript. Then the equations of auxiliary pressure, stream function, streamwise momentum and energy in terms of the $\bar{f}$ functions are

$$\bar{p} = (\gamma-1)\int_0^\infty \bar{f}_1\, \mathrm{d}\zeta/(4\gamma C_3)^{1/2}, \tag{3.11}$$

$$\psi_\zeta - \bar{u}\bar{\delta} = 0, \tag{3.12}$$

$$4\bar{p}^2\bar{u}_{\zeta\zeta} + \psi\bar{\delta}\bar{p}\bar{u}_\zeta + \gamma_1\bar{\delta}^2\bar{f}_1\bar{p} + 4\xi\bar{\delta}(\bar{p}\psi_\xi\bar{u}_\zeta - \bar{\delta}\bar{p}\,\bar{u}\bar{u}_\xi - \tfrac{1}{2}\gamma_1\bar{f}_1\bar{\delta}\bar{p}_\xi) = 0, \tag{3.13}$$

$$Pr_1\bar{p}(\bar{u}\bar{u}_\zeta)_\zeta + \bar{p}\bar{H}_{\zeta\zeta} + \tfrac{1}{4}Pr\,\psi\bar{\delta}\bar{H}_\zeta + \xi\,Pr\,\bar{\delta}(\bar{H}_\zeta\psi_\xi - \bar{u}\bar{\delta}\bar{H}_\xi) = 0, \tag{3.14}$$

respectively, where $\gamma_1 = (\gamma-1)/\gamma$, $\bar{f}_1 = \frac{3}{4}\eta\bar{u}\bar{\delta} - \bar{v}$ and $Pr_1 = Pr - 1$. Similarly in the inviscid layer, the equations of continuity, transverse momentum, and energy are

$$\bar{f}_2\bar{\rho}_\eta + 4\bar{\rho}\bar{v}_\eta + 4\xi(\bar{f}_3\bar{\rho}_\xi + \bar{f}_4\bar{\rho}_\eta) = 0, \tag{3.15}$$

$$\bar{f}_2\bar{\rho}\bar{v}_\eta + 4\bar{p}_\eta - \bar{f}_3\bar{v}\bar{\rho} + 4\xi\bar{\rho}(\bar{f}_3\bar{v}_\xi + \bar{f}_4\bar{v}_\eta) = 0, \tag{3.16}$$

$$\bar{f}_2(\bar{\rho}\bar{\rho}_\eta - \gamma\bar{p}\bar{\rho}_\eta) - 2\bar{f}_3\bar{\rho}\bar{p} + 4\xi[\bar{f}_3(\bar{\rho}\bar{p}_\xi - \gamma\bar{p}\bar{\rho}_\xi) + \bar{f}_4(\bar{\rho}\bar{p}_\eta - \gamma\bar{p}\bar{\rho}_\eta)] = 0, \tag{3.17}$$

respectively, where $\bar{f}_2 = 4\bar{v} + 3(\eta-1)\bar{\delta} - 3C_5\eta\bar{g}$, $\bar{f}_3 = C_5\bar{g} - \bar{\delta}$ and $\bar{f}_4 = (\eta-1)\bar{\delta}_\xi - C_5\eta\bar{g}_\xi$. The boundary conditions at the wall and the boundary-layer edge are

$$\bar{u} = 0, \quad \psi = 0, \quad \bar{H}_\zeta = 0 \quad \text{or} \quad H = H_w \tag{3.18}$$

$$\bar{u} = 1, \quad \bar{H} = \tfrac{1}{2}. \tag{3.19}$$

However, the boundary-layer edge condition on the transverse velocity, that is $\bar{v} = \frac{3}{4}\bar{\delta} + \xi\bar{\delta}_\xi$, is disregarded, as it is satisfied automatically. At the shock wave the conditions for the transverse velocities, pressure and density are

$$\bar{v}_s = \frac{2}{\gamma+1}\left(\bar{g}_1 - \frac{\bar{\chi}_1}{\bar{g}_1}\right), \quad \bar{p}_s = \frac{2}{\gamma+1}\left(\bar{g}_1^2 - \frac{\gamma-1}{2\gamma}\bar{\chi}_1\right), \quad \bar{\rho}_s = \frac{\gamma+1}{\gamma-1}\left(1 + \frac{2}{\gamma-1}\frac{\bar{\chi}_1}{\bar{g}_1^2}\right)^{-1}, \tag{3.20}$$

defining $\bar{g}_1 = C_5(\frac{3}{4}\bar{g} + \xi\bar{g}_\xi)$ and $\bar{\chi}_1 = \xi^{1/2}/\chi^3 C_2^2$.

The two systems of parabolic and hyperbolic nonlinear partial differential equations in the viscous and inviscid layers respectively, with their boundary conditions, i.e. (3.11)–(3.20), may be solved simultaneously for a given value of the wall enthalpy by

a forward-marching approach using a Crank–Nicolson implicit finite-difference method with relaxation to determine the flow variables and the positions of the boundary-layer edge and the shock wave, with matching at the boundary-layer edge. However, before the process of marching downstream can be started accurate initial profiles are required in both layers. These can be obtained by reducing the above partial differential equations to the ordinary similarity ones holding near the leading edge, where ξ approaches zero and consequently the functions $\bar{\delta}$, $\bar{p}$ in the viscous layer and $\bar{g}$ approach unity.

In the present numerical approach, the transverse distance from the wall to the boundary-layer edge and from the latter to the shock wave, and the streamwise distance from the leading to the trailing edge, are covered by $J-2$, $I-2$ grid points with step widths of h, w, respectively. Thus $2 \leqslant j \leqslant J$, $2 \leqslant i \leqslant I$, as presented in figure 3. In the viscous layer all functions are averaged, and their derivatives replaced by the central differences, with respect to the $(i-\frac{1}{2}, j-\frac{1}{2})$ point in (3.12), and to the $(i-\frac{1}{2}, j)$ point in (3.13), (3.14); but in the inviscid layer (3.15)–(3.17) the discretization is with respect to the first point. This process is carried on with respect to the point $(i-\frac{1}{2}, J)$ for the pressure and the boundary-layer thickness in the viscous layer, and in the inviscid layer with respect to $(i-\frac{1}{2}, 1)$ and $(i-\frac{1}{2}, J)$ for the boundary-layer thickness and the shock shape, respectively, since they are dependent on streamwise distance only. Assuming that all flow variables $\bar{f}$, C_5 in the inviscid layer are such that $\bar{f} = \hat{f} + \check{f}$, where $\check{f} \ll 1$, a linearized system is obtained which can be written as algebraic equations in the form

$$(\ldots)\check{f}_{i,j-1} + (\ldots)\check{f}_{i,j} + (\ldots)\check{f}_{i,j+1} + (\ldots) \underset{\text{in VL}}{\check{p}_i} \quad \text{or} \quad \underset{\text{in IL}}{\check{g}_i} = \text{R.H.S.} \Rightarrow \boldsymbol{A}\check{\boldsymbol{f}} = \boldsymbol{R}. \tag{3.21}$$

The coefficients of the $\check{f}$ and the right-hand side are functions of $\hat{f}$, $\boldsymbol{A}$ is a $(n+1) \times (n+1)$ matrix with $n = 3J$ elements, and $\check{\boldsymbol{f}}$, $\boldsymbol{R}$ are column vectors. At each streamwise step i on the boundary-layer edge (represented by • in figure 2), an initial guess is made for the position of the boundary-layer edge and the flow variables along the transverse steps j in either layer; then the vector $\check{\boldsymbol{f}}$ is computed repeatedly by applying forward Gaussian elimination of the upper diagonal elements of the matrix $\boldsymbol{A}$ without the $n+1$ column and row, until $\check{f}$ approaches the required solution $\bar{f}$ (that is $\hat{u} \to \bar{u}$, etc.). For example, for accuracy of 0.1×10^{-14} between ten and twenty iterations are needed. Then, by using these values and predicting a more accurate value for the position of the boundary-layer edge through an iterative procedure, the process of computing the new values using the old values as initial guesses is continued until the pressure difference at the boundary-layer edge determined from each layer approaches a suitably small value, indicating that the pressure is matched. About twelve iterations are required if this small value is 0.1×10^{-10}. It is then automatic that the transverse velocity and the other flow variables match exactly or asymptotically on or approaching the boundary-layer edge from each layer.

With the solution thereby determined at this step i, the process of marching downstream in a similar way continues towards the trailing edge, with the computed i-values used as initial guesses for the step $i+1$. Concerning the computation of the initial profiles, in the viscous layer $\hat{H} = \frac{1}{2} + \zeta^2 \mathrm{e}^{-2\zeta}$, $\hat{u} = 1 - \mathrm{e}^{-2\zeta}$, $\hat{\psi} = \zeta + \frac{1}{2}(\mathrm{e}^{-2\zeta} - 1)$, and in the inviscid layer $\hat{C}_5 = \frac{3}{2}$, $\hat{v} = \frac{3}{4}(1-\eta) + \frac{3}{2}\hat{C}_5\,\eta(\gamma+1)$, $\hat{\rho} = \eta(\gamma+1)/(\gamma-1)$, $\hat{p} = \frac{9}{8}\hat{C}_5^2\,\eta(\gamma+1)$, are used as initial guesses. They satisfy the relevant boundary conditions at the wall, boundary-layer edge and/or shock wave, and result in a convergence rate below that found downstream. The unknown constants C_3, C_5 in (3.9), (3.10) are determined during the computation of the initial profile in the viscous layer by applying the

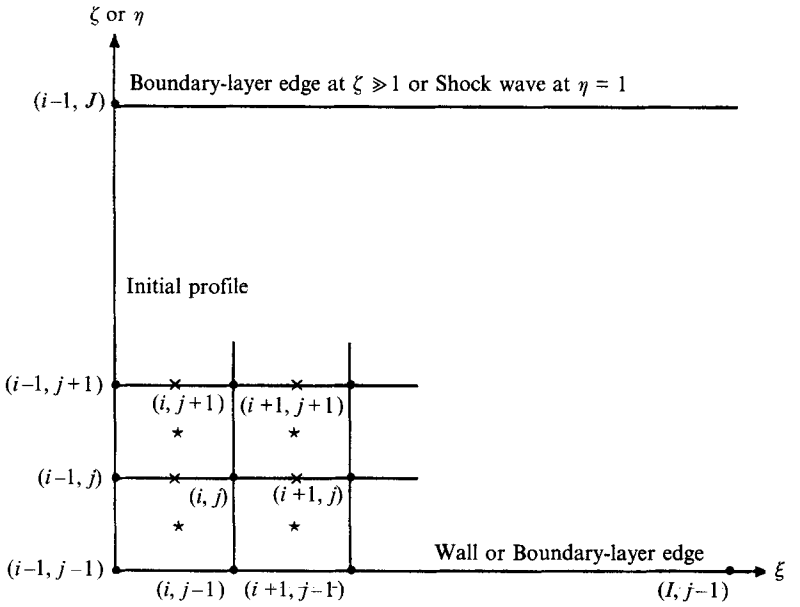

FIGURE 3. Typical mesh structures for finite-difference computations.

Wall enthalpy	C_1	C_2	C_4
0.01	0.103219, 0.115688	0.359295, 0.380377	0.607733, 0.643393
0.05	0.130235, 0.139532	0.403584, 0.417742	0.682647, 0.706594
0.10	0.163658, 0.169056	0.452417, 0.459818	0.765246, 0.777764
0.30	0.293925, 0.284331	0.606302, 0.596325	1.025535, 1.008660
Insulated	0.368429, 0.395719	0.678810, 0.703500	1.148179, 1.189943

TABLE 1. Values of constants C_1, C_2 and C_4 in (3.9) and (3.10) for $Pr = 0.725$, unity

trapezoidal rule to the auxiliary pressure equation (3.11) and inviscid layer respectively. Then, since the pressure should be matched at the boundary-layer edge, by equating the pressure in the two layers using (3.9), (3.10) the constant C_2 is determined as $C_2 = [CC_3/\bar{p}^{IL}_{(j=1)}]^{1/4}$. The values of these constants in (3.9), (3.10) for Prandtl numbers of 0.725 and unity, at different values of the wall enthalpy, are given in table 1. The values of enthalpy for the insulated wall are 0.4178, 0.5 for Prandtl numbers of 0.725, unity respectively, and C_5 is 1.691460. For the insulated wall and Prandtl number of unity, Stewartson (1955) determined the value of C_1 to be 0.394, and Oguchi (1958) computed the values of C_1, C_2 as 0.396, 0.704 respectively. These are in agreement with the computed values here. A Runge–Kutta method with error of order h^5 was used to compute the initial profile in the inviscid layer, where the results were in agreement to more than six decimal places with the previous method. Owing to the explicit nature of the numerical method and the curved shock wave near the leading edge, however, the process of marching downstream seemed to be successful only for a relatively short streamwise distance if the Runge–Kutta method was applied, so the previous approach was used again.

The computational results show that, for high values of the hypersonic interaction parameter, the values of the viscous-layer variables downstream effectively approach

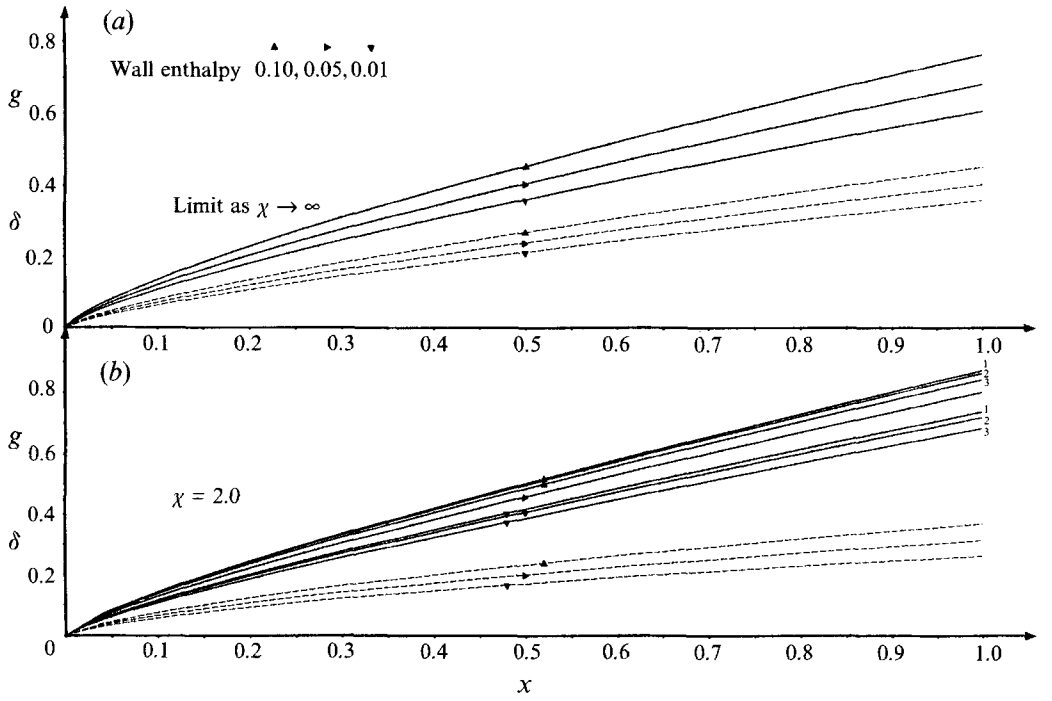

FIGURE 4. The positions of the shock wave g (——) and the boundary-layer edge δ (------), using forward-marching single-sweep method with no upstream influence and (b) comparisons with the NS and PNS methods (curves 1, VL–IL method; 2, NS; 3, PNS; for $M_\infty = 16$, $Re_\infty = 8^6$) (see §3). For the wall enthalpy of 0.1 the numerical values of the shock wave using the VL–IL and NS methods (curves 1 and 2) almost coincide. The streamwise distances of zero and unity indicate the leading edge and the trailing edge: $Pr = 0.725$.

the initial-profile values, that is the similarity solution is preserved. The positions of the boundary-layer edge δ, the shock wave g, the pressure p at the boundary-layer edge, and at different streamwise distances from the leading edge in the inviscid layer, are presented in figures 4 and 5 for different values of the constant wall enthalpy, the hypersonic interaction parameter versus streamwise distance, and Prandtl number 0.725. The step sizes h are 0.02 in the viscous layer, using 501 points from the wall to the boundary-layer edge with the stretched coordinate ζ chosen to be 10, and 0.01 in the inviscid layer, using 101 points from the boundary-layer edge to the shock wave, while the streamwise step w is 0.01 using 101 points from the leading to the trailing edge. Details of the computational procedure, such as the final forms of the algebraic equations, the matrix handling and the iteration methods, are complicated and are shown in Khorrami (1991).

In particular, the positions of the shock waves are in excellent and reasonable agreement with results provided by J. J. Korte (1993, personal communication) from the numerical solutions of the Navier–Stokes and the parabolized Navier–Stokes equations respectively, as presented in figure 4, for $M_\infty = 16$ and $Re_\infty = 8^6$ (that is $\chi = 2$), and $T_w^*/T_\infty^* = 10.24$ and 1.024 (corresponding to $H_w = 0.1$ and 0.01 respectively). Korte's computations captured the shock positions by using explicit second-order upwind schemes, for integrating the Navier–Stokes and the parabolized Navier–Stokes equations (with further use of Vigneron's technique of splitting the streamwise pressure gradient, for the parabolized Navier–Stokes equations).

The streamwise velocity u^* in the inviscid layer is approximately the same as the free-

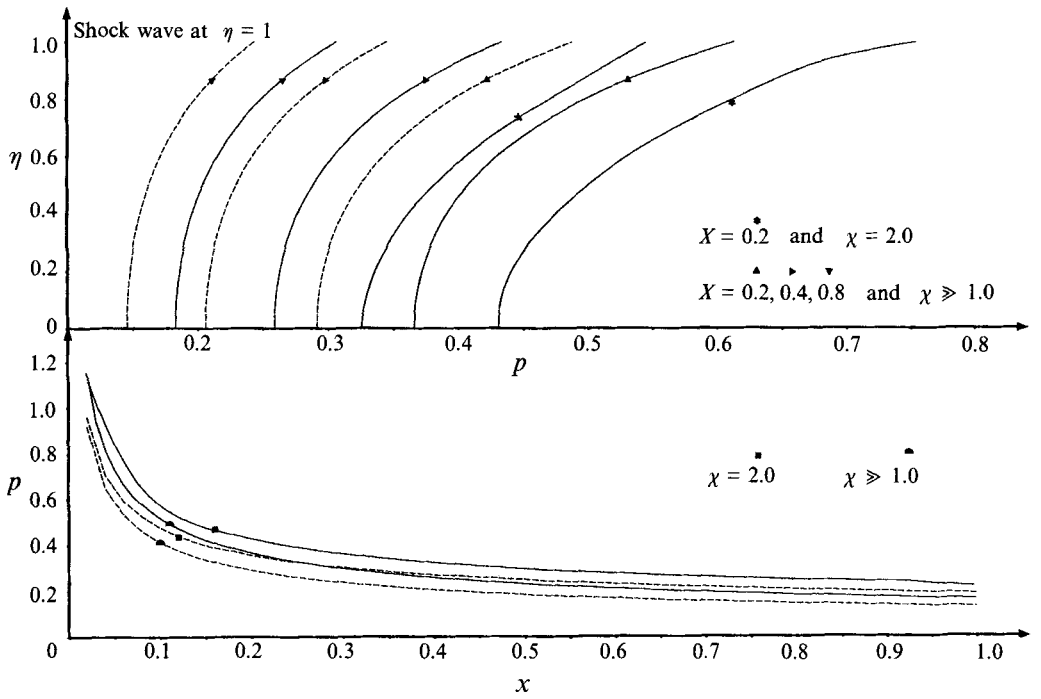

FIGURE 5. Pressure p at the boundary-layer edge and at different streamwise distances from the leading edge (see §3 and figure 4): $Pr = 0.725$; ——, wall enthalpy = 0.10; – – –, 0.05.

stream velocity U^* and consequently the non-dimensional u representing a negative deficit is negligible, being of order ϵ^2 according to (2.11). Similarly the enthalpy is also negligible. The scaled deficit, $-u$, tends to infinity as the lower bound of the inviscid layer is approached, in readiness for matching with the boundary layer where the deficit is no longer negligible and the singular behaviour at the boundary-layer edge follows from the governing equations. The matching strictly also involves the thinner entropy layer, near the boundary-layer edge, which can alter the precise manner in which u tends towards minus infinity; however, the entropy layer is negligible here. The scaled density approaches infinity or zero on the boundary-layer edge, in the viscous or inviscid layer respectively, as expected theoretically from (2.11). At high values of the interaction parameter, the density profile downstream in the inviscid layer does not change, as it is then independent of the streamwise distance and the value of wall enthalpy. For, at the boundary-layer edge, the function $\bar{\delta}(x)$ approaches unity regardless of the wall enthalpy, and on the shock wave the density has the constant value of 6, from (3.20). However, as the function $\bar{\delta}(x)$ changes downstream, such as on an airfoil, the density profile downstream changes for high values of the interaction parameter.

As the wall enthalpy increases, for a given hypersonic interaction parameter χ or free-stream Mach number, the thickness of the viscous layer and consequently of the shock layer increases; but as χ increases, for a given wall enthalpy, the thickness of the shock layer decreases while the viscous layer becomes thicker, as shown in figure 4 and also according to theoretical expectation. At high values of the interaction parameter, as $\chi \to \infty$, the value of $\bar{\delta}(x)$ approaches unity and the position of the boundary-layer edge from (3.9) for a particular wall enthalpy can be computed as $C_2 x^{3/4}$, without the process of marching downstream towards the trailing edge. Downstream, however, a major point is that the forward-marching solution in the viscous layer departs from the

main (required) solution at different streamwise distances from the leading edge, depending on the wall enthalpy H_w, the interaction parameter and the streamwise step size. This phenomenon of *branching* and *free interaction* is known to be due to the presence of upstream influence, which in fact is able to affect the flow properties on the global scale right up to the leading edge. As the value of the wall enthalpy decreases from its insulated value, on the other hand, the effect of upstream influence reduces and branching in the streamwise direction is delayed, for given values of the interaction parameter and the streamwise step size. The branching effect tends to be negligible for the lower values of wall enthalpy, $H_w \leqslant 0.1$ apparently, whereas low values of the interaction parameter and the streamwise step size expedite this nonlinear breakdown. At high values of the interaction parameter and low values of wall enthalpy, it is found that the viscous and inviscid layers can be solved simultaneously all the way from the leading to the trailing edge, for a wide range of step sizes, with the effect of upstream influence approximately remaining almost insignificant; but as the interaction parameter decreases, for the same values of wall enthalpy and step size, this process of matching and marching downstream is severely hindered since the effect of upstream influence appears to become significant within a relatively short streamwise distance of the leading edge. This is discussed by Khorrami *et al.* (1989), and Brown *et al.* (1991). Furthermore, the streamwise distance from the leading edge required for the branching effect to become significant decreases as the interaction parameter decreases, for a given value of wall enthalpy and step size, since the dimensional distance x^* is proportional to $\chi^6 x$. Therefore, at any value of the wall enthalpy and the interaction parameter, the nonlinear breakdown can be delayed or expedited, and consequently the streamwise distance from the leading edge, for the branching to start, can be increased or decreased as the value of the streamwise step size is increased or decreased respectively. Thus, for a particular value of the wall enthalpy, as the interaction parameter is decreased the step size should be increased to delay the nonlinear breakdown. On the other hand, the computational results show that larger values of the step size introduce numerical errors in the inviscid layer, and in particular the results tend to oscillate near the shock wave, although the results in the viscous layer are little affected. Furthermore, numerical instability is almost certainly not the cause of the oscillation (see §4), the magnitude of the oscillation decreases as the step size is reduced, but the step size cannot be reduced too far without affecting the nonlinear breakdown. These findings prompted the work of the next three sections.

4. Hypersonic upstream influence

Non-uniqueness of the solution near the leading edge of an insulated sharp flat plate in hypersonic flow, due to upstream influence, was discovered by Neiland (1970), using the tangent-wedge method to describe the inviscid layer. Later Werle, Dwoyer & Hankey (1973) considered the non-insulated wall also. This non-uniqueness is associated with a single eigenvalue and eigenfunction occurring between the fifty-first and fifty-second term of the series expansion (see §3) of the pressure, in terms of powers of the classical interaction parameter, for an insulated wall with Prandtl number of unity and γ of 1.4. Brown & Stewartson (1975), using the inviscid layer equations of motion, then concluded that the tangent-wedge method is extremely accurate. This eigenfunction is due to the interaction of the viscous and inviscid layers, and is closely analogous with the eigenfunction in supersonic flow discussed by Lighthill (1953) and Stewartson & Williams (1969).

In the viscous layer, the equation of continuity (2.12) is satisfied if the stream

function $\psi(x,y)$ is chosen such that $\partial\psi/\partial x = -\rho v$ and $\partial\psi/\partial x = \rho u$. Then, by transforming the y-variable to z, such that

$$0 \leqslant z = \int_{\tau(x)}^{y} \rho \, \mathrm{d}y < \infty,$$

where $\tau(x)$ gives the wall shape (zero for a flat plate), the governing equations from (2.13)–(2.17) are

$$\tilde{\psi}_z = \tilde{u}, \tag{4.1}$$

$$\tilde{\psi}_z \tilde{\psi}_{xz} - \tilde{\psi}_x \tilde{\psi}_{zz} = C\gamma\tilde{p}\tilde{\psi}_{zzz} - (\gamma-1)(2\tilde{H}-\tilde{u}^2)\tilde{p}_x/2\gamma\tilde{p}, \tag{4.2}$$

$$\tilde{\psi}_z \tilde{H}_x - \tilde{\psi}_x \tilde{H}_z = C\gamma\tilde{p}[(\tilde{H}_z/Pr) + (1-1/Pr)\tilde{\psi}_z\tilde{\psi}_{zz}]_z, \tag{4.3}$$

$$\tilde{\delta}(x) = \tilde{\tau}(x) + (\gamma-1)\int_0^\infty (2\tilde{H}-\tilde{u}^2)\,\mathrm{d}z/2\gamma\tilde{p}, \tag{4.4}$$

where the differentiation is with respect to the subscript. Next the variable z is transformed to $\hat{\eta}$ such that $0 \leqslant \hat{\eta} = x^{-1/4}z < \infty$, and the following asymptotic expansion about the leading edge,

$$\hat{f} = x^m(\hat{f}_o + x^{1/2}\hat{f}_1 + x\hat{f}_2 + \ldots + x^{n/2}\hat{f}_n + x^\alpha \hat{f}_e + x^{(n+1)/2}\hat{f}_{n+1} + \ldots), \tag{4.5}$$

is substituted into (4.1)–(4.4). The appropriate powers of x yield two separate sets of ordinary differential equations, namely the base- and eigen-flow equations. The constant m is 0, $\frac{1}{4}$, 0, $-\frac{1}{2}$, $\frac{3}{4}$, $\frac{3}{4}$, when $\hat{f}$ represents $\hat{u}$, $\hat{\psi}$, $\hat{H}$, $\hat{p}$, $\hat{\delta}$, $\hat{\tau}$, and the $\hat{f}_n$ depend on $\hat{\eta}$ but are constant when $\hat{f}$ represents $\hat{p}$, $\hat{\delta}$, $\hat{\tau}$, in which case the right-hand side should be multiplied by $1/C\gamma$, C and C respectively. Here α is the unknown eigenvalue, such that $n < 2\alpha < n+1$, and the subscript e indicates the eigenfunction or term. The eigenvalue is independent of the precise geometry of the source of the disturbance downstream, only the coefficients of the expansions differing from one case to another. In particular, the base- and eigen-equations for the boundary-layer edge position are

$$\hat{\delta}_o = \hat{\tau}_o + \frac{\gamma-1}{2\hat{p}_o}\int_0^\infty (2\hat{H}_o - \hat{u}_o^2)\,\mathrm{d}\hat{\eta}, \quad \hat{\delta}_e = (\hat{\tau}_o - \hat{\delta}_o)\frac{\hat{p}_e}{\hat{p}_o} + \frac{\gamma-1}{\hat{p}_o}\int_0^\infty (\hat{H}_e - \hat{u}_o\hat{u}_e)\,\mathrm{d}\hat{\eta},$$

respectively. Then by putting

$$\hat{\eta} = 2\hat{p}_o^{1/2}\eta, \quad \hat{\tau}_o = (\gamma-1)\frac{\tau_o}{\hat{p}_o^{1/2}}, \quad \hat{\delta}_o = (\gamma-1)\frac{\delta_o}{\hat{p}_o^{1/2}}, \quad \hat{\delta}_e = \frac{\gamma-1}{2(2\alpha+1)}\frac{\hat{p}_e\delta_e}{\hat{p}_o^{3/2}},$$

$$\hat{u}_e = \frac{\alpha+1}{2\alpha+1}\frac{\hat{p}_e}{\hat{p}_o}\left(2u_e - \frac{\eta u_o'}{2\alpha+2}\right), \quad \hat{H}_e = \frac{\alpha+1}{2\alpha+1}\frac{\hat{p}_e}{\hat{p}_o}\left(2H_e - \frac{\eta H_o'}{2\alpha+2}\right),$$

with $\hat{u}_o$, $\hat{H}_o$ remaining unchanged, the base- and eigen-flow equations for the boundary-layer edge are normalized as

$$\delta_o = \tau_o + \mathscr{I}_o, \quad \delta_e = (4\alpha+1)(\tau_o - \delta_o) + 8(\alpha+1)\mathscr{I}_e,$$

where it can be shown that

$$\mathscr{I}_o = \int_0^\infty (2H_o - u_o^2)\,\mathrm{d}\eta, \quad \mathscr{I}_e(\alpha) = \int_0^\infty (H_e - u_o u_e)\,\mathrm{d}\eta.$$

The pressure terms can be determined by the tangent-wedge method using (2.25), (4.5) as

$$\hat{p}_o = 9C^3\gamma(\gamma+1)\hat{\delta}_o^2/32, \quad \hat{p}_e = 3C^3\gamma(\gamma+1)(4\alpha+3)\hat{\delta}_o\hat{\delta}_e/16,$$

resulting in a relationship between the base- and eigen-terms of the boundary-layer edge, which yields the expression for the eigenvalue α in the form

$$4(4\alpha+3)\mathscr{I}_e-(8\alpha+3)\mathscr{I}_o = 3(2\alpha+1)\tau_o/2(\alpha+1). \tag{4.6}$$

Since this usually has a solution, upstream influence exists, although its effect depends on the eigenvalue. The eigenvalue α is typically large, for example approximately 50 for a Prandtl number of unity, wall enthalpy of 0.5 and γ of 1.4, as determined by Neiland (1970), and is proportional to H_w^{-6} at small values of wall enthalpy as shown by Brown & Stewartson (1975). Therefore the eigenvalue increases or decreases with decreasing or increasing H_w, causing less or more upstream influence respectively. The earlier computational results confirm that, as the wall enthalpy increases towards its insulated value, the upstream influence becomes more severe and speeds up the branching behaviour, i.e. the departure from the main solution. The inviscid layer can be analysed to determine the eigen-term of the pressure in particular, as an alternative to using the tangent-wedge approximation; however, use of the tangent-wedge method, i.e. using (4.6) for the purpose of testing on upstream influence, is accurate (see details in Khorrami 1991).

Further analytical study of the combined effect of *velocity slip* and *enthalpy jump* at the wall on upstream influence, shown by Khorrami (1991), indicates that there is no upstream influence near the leading edge then, meaning that with velocity slip the solutions do not branch downstream, regardless of the value of the wall enthalpy. There is concern also with the effect of increasing body thickness on the eigenvalue α; again detailed analysis is shown by Khorrami (1991). For bodies of relatively large thickness (that is large τ_o), it can be shown that α must be large for (4.6) to be balanced, since $\mathscr{I}_o$ is usually of order unity except for hot or cold walls and Newtonian–Busemann flows where $\gamma \approx 1$, which in turn affect $\mathscr{I}_e$. It can be shown that

$$\alpha \approx \frac{3}{16}\frac{\tau_o}{\mathscr{I}_e} = -\frac{27}{128}\frac{\lambda^{5/4}}{H_w^{3/2}}\left[\frac{\gamma\tau_o\,\mathrm{Ai}'(0)}{\gamma-1}\right]^{3/4}, \tag{4.7}$$

where λ is the skin friction coefficient and Ai is the Airy function. Therefore, α is proportional to $H_w^{-3/2}$ and $[\tau(x)]^{3/2}$, which contrasts with H_w^{-6} for thin bodies such as a flat plate. The nature of this upstream influence is important for applications to real airfoil shapes; see also §6.

5. Hypersonic viscous flow with upstream influence

The analytical and computational work above shows that, as the wall enthalpy increases towards its insulated values of 0.4178, 0.5 for Prandtl numbers of 0.725, unity respectively, nonlinear breakdown occurs rapidly at different streamwise distances in the viscous layer. This is due to branching, and departure from the main solution, as the eigen-terms in the series expansion near the leading edge (see §4) become more significant. Consequently, the shock layer cannot be computed by a forward-marching method up to the trailing edge in general (see also §7). Below, the viscous layer is solved numerically between the leading and trailing edges by two independent computational methods; multiple sweeps are applied, such that the initial condition upstream and the

end pressure condition downstream are satisfied at each sweep and an overall converged solution is obtained during the final sweep. These methods, using the tangent-wedge relation first for convenience, accommodate the branching but are designed to prevent nonlinear breakdown, and they directly bring in the effect of the upstream influence as required.

First the *nonlinear sweeps* (NLS) method is based on the previous treatment of the hypersonic shock layer in §3. The initial profile and the far-downstream pressure, applied here at the trailing edge ($p_{(I)} \to 1/\gamma\chi^3$, using (3.1), (3.8), (2.25) and noting that here as $x \to 1$ the slope of the boundary-layer edge is taken as $\mathrm{d}\delta/\mathrm{d}x \to 0$), are kept unchanged during each sweep, marching downstream from the leading to the trailing edge with local nonlinear updating. The use of trailing edge as the most downstream station is explained in the next paragraph. More significantly, however, $\bar{p}(\xi)$ is now forward-differenced to bring in the upstream influence directly, and $\bar{\delta}(\xi)$ in (3.8) is replaced by the expression from the tangent-wedge approximation (2.25). The constant C_2 is determined as before, through solving and matching the initial profiles of the viscous and inviscid layers. In the first sweep, the trailing-edge value of $\bar{p}_{(I)}$ is used as the initial guess for $\bar{p}_{(i)}$ at all points, except in the initial profile, to determine the value of $\bar{\delta}_{(i)}$ at the corresponding points. Then downstream marching is performed during the computation of the shock layer, from the first station after the initial profile to the station immediately before the trailing edge. The new values of the $\bar{p}_{(i)}$ determined from the first sweep are used as the initial guess for the second sweep, and the same procedure is repeated until $[p_{(i)}]^n - [\bar{p}_{(i)}]^{n-1} \to 0$ becomes suitably small from the computational point of view for $2 \leqslant i < I$, where n is the number of the sweep.

Secondly, the *linear sweeps* (LS) method instead incorporates nonlinearity via global Newton-iteration updates of the complete flow field, rather than nonlinear sweeping and local nonlinear updating. The variables x, z are replaced by $-\infty \leqslant \xi = \ln x \leqslant 0$, $0 < \eta = z\,\mathrm{e}^{-\xi/4} \to \infty$, so that the leading and trailing edges are transformed to minus infinity and zero respectively, and the transverse coordinate is stretched to infinity. Then, by setting

$$\tilde{\psi} = \mathrm{e}^{\xi/4}\,\bar{\psi}(\xi,\eta), \quad \tilde{p} = \bar{p}(\xi)/C\gamma\,\mathrm{e}^{\xi/2}, \quad \tilde{\delta} = C\,\mathrm{e}^{3\xi/4}\,\bar{\delta}(\xi), \quad \tilde{\tau} = C\bar{\tau}(\xi), \tag{5.1}$$

and leaving the streamwise velocity and enthalpy unchanged, the controlling equations from (4.1)–(4.4) become

$$\left.\begin{aligned} &\bar{\delta} = \bar{\tau} + (\gamma-1)\int_0^{\eta} (2\bar{H}-\bar{u}^2)\,\mathrm{d}\eta/2\bar{p}, \quad \bar{\psi}_\eta - \bar{u} = 0, \\ &\bar{u}\bar{u}_\xi - (\bar{\psi}_\xi + \tfrac{1}{4}\bar{\psi})\,\bar{u}_\eta = \bar{p}\bar{u}_{\eta\eta} - (\gamma-1)\,(2\bar{H}-\bar{u}^2)\,[\bar{p}'(\xi) - \tfrac{1}{2}\bar{p}]/2\gamma\bar{p}, \\ &\bar{u}\bar{H}_\xi - (\bar{\psi}_\xi + \tfrac{1}{4}\bar{\psi})\,\bar{H}_\eta = \bar{p}[\bar{H}_{\eta\eta} + (Pr-1)\,(\bar{u}\bar{u}_\eta)_\eta]/Pr. \end{aligned}\right\} \tag{5.2}$$

The flow solution is independent of ξ as the leading edge is approached, provided the body is not too blunt and its thickness τ is of order $x^{3/4}$ or $\mathrm{e}^{3\xi/4}$, at most, as $x \to 0$ or $\xi \to -\infty$ respectively, and the similarity form holds. The main boundary conditions are

$$\bar{u} = 0, \quad \psi = 0, \quad \bar{H} = H_w; \qquad \bar{u} = 1, \quad \bar{H} = \tfrac{1}{2}. \tag{5.3}$$

The typical solution quantity $\bar{f}(\xi,\eta)$ is to be taken the sum of a global guess $\hat{f}(\xi,\eta)$ and a small correction term $\check{f}(\xi,\eta)$ (e.g. $\bar{u} = \hat{u} + \check{u}$), so that governing equations may be linearized. For example the stream-function equation becomes $\check{u} - \check{\psi}_\eta = \hat{\psi}_\eta - \hat{u}$. The discretization of the complete linearized system is similar to that discussed for the hypersonic shock layer. However, the functions in the equation of continuity are

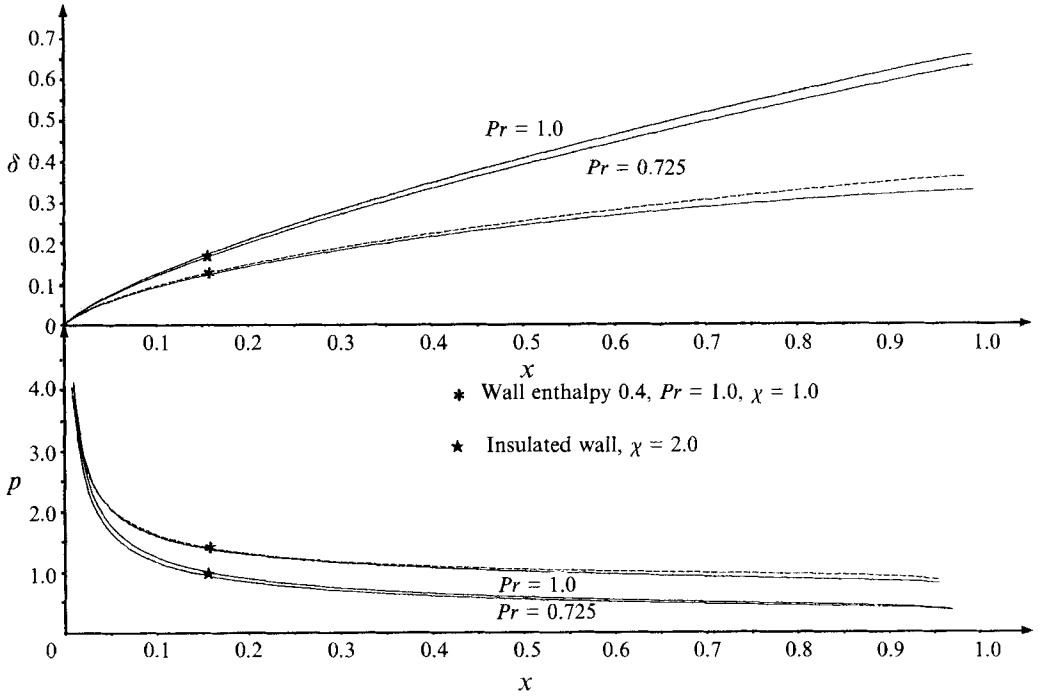

FIGURE 6. Boundary-layer edge position δ and pressure p, for high values of wall enthalpy with upstream influence, using multi-sweeps methods (see §5): ——, NLS; – – –, LS.

averaged and their derivatives replaced by two-point differences centred with respect to the $(i,j-\frac{1}{2})$ point, the streamwise-pressure-gradient term is forward-differenced again, to suppress the branching, and the term δ is replaced by the expression for the streamwise slope of the boundary-layer edge using (2.25). Then the algebraic form of these equations is solved by repeated forward and backward linear sweeps between the leading edge and the most downstream station, representing downstream infinity (see later). The required conditions at that station (i.e. pressure $1/\gamma\xi^3$) and at the leading edge are imposed during each sweep. The sweeping is continued until the pressure correction is converged. A new global guess follows and the process of linear sweeping is applied as above; then this procedure is repeated, until overall convergence is achieved. The method is second-order-accurate nominally, except for the pressure gradient. Again, the computational procedures are quite complicated and are shown by Khorrami (1991). Smith & Khorrami (1991) used a modified LS method simultaneously to investigate the supersonic regime, for interactive separating flow past a ramp according to triple-deck theory, for comparison. The particular linear shooting procedure used within their modified method was found to have limited success in the present context except for relatively short streamwise lengths, owing to the rapidity of the branching. In similar vein, moving the most downstream station in the present computations upstream, even as far as the trailing edge, had very little influence on the bulk of the solution obtained on the body.

The pressure and the boundary-layer edge position are presented in figure 6 for an insulated wall, Prandtl numbers of 0.725 and unity and an interaction parameter of two, using the NLS method. Furthermore, the NLS and LS methods are compared with each other, for Prandtl number and interaction parameter of unity and wall enthalpy of 0.4 (see figure 7 for the convergence history of the pressure). In the NLS

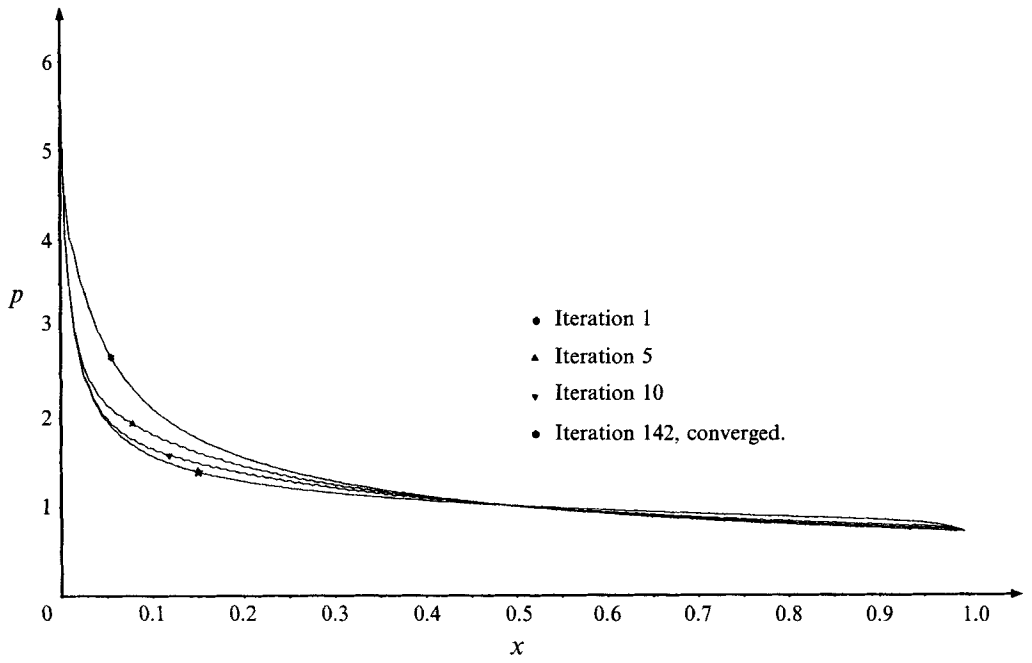

FIGURE 7. Convergence history of pressure on the boundary-layer edge using NLS method (see §5): wall enthalpy 0.4, $Pr = 1.0$, $\chi = 1.0$.

method, the step sizes in the transverse and streamwise directions are 0.02 (501 points from the wall to the boundary-layer edge, with the stretched coordinate equal to 10) and 0.005 (201 points from the leading to the trailing edge). Comparable step sizes were required in the LS method, although there the streamwise transformed grid points are spaced non-uniformly with a higher resolution near the leading edge. Approximately 150 and 200 sweeps with an accuracy of 0.1×10^{-9} and 0.1×10^{-6} are needed for the overall pressure convergence in the NLS and LS methods respectively.

6. Hypersonic flow over thin airfoils

The LS method was readily extended to compute the hypersonic interactive flow over thin airfoils where $\tau \neq 0$, with minor modifications. Wall enthalpies close to the insulated value, which is 0.5 for Prandtl number of unity, were taken, and the LS method incorporated upstream influence using the tangent-wedge approximation. Airfoils with contours $\tau(x)$ such as

$$\tau = c_1 x^{3/4} x^{c_2}/(1 + c_3 x^{c_4}) \quad \text{for} \quad 0 < x < \infty \quad (\text{with} \quad c_2 + \tfrac{3}{4} < c_4) \tag{6.1}$$

were considered, where c_1, c_2, c_3, c_4 are constants such that $\tau > 0$ and $\tau(\infty) = 0$. Their maximum and trailing-edge thicknesses τ_M, τ_T occur at distances x of c^{1/c_4}, unity and are

$$\tau_M = c_1 \frac{c^{(c_2+3/4)/c_4}}{1 + c_3 c}, \quad \tau_T = \frac{c_1}{1 + c_3}, \quad \text{with} \quad c = \frac{4c_2 + 3}{c_3(4c_4 - 4c_2 - 3)}, \tag{6.2}$$

respectively. In particular, the pressure and the boundary-layer edge were determined for airfoils with contours

$$\tau_1 = 3(98)^{1/3} x/40(1 + 49x^3), \quad \tau_2 = 2\tau_1, \tag{6.3}$$

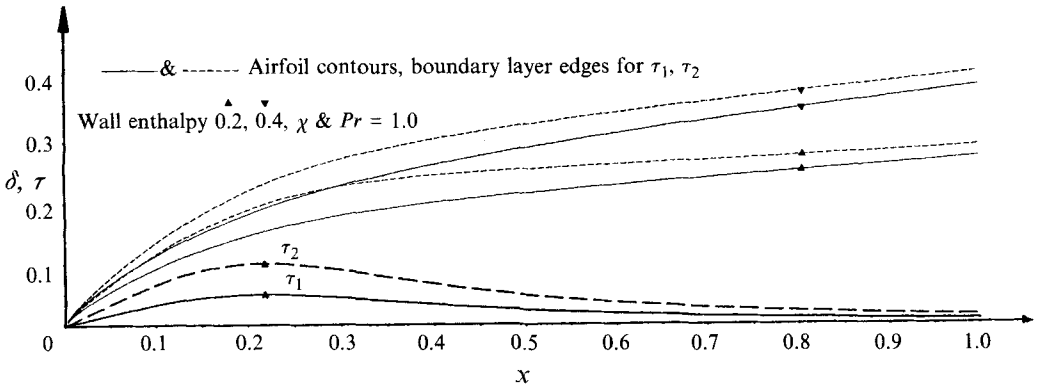

FIGURE 8. Boundary-layer edge positions δ, for airfoils in viscous hypersonic flow with upstream influence using LS method (see §§6, 5).

by choosing c_1, c_2, c_3, c_4 as $3(2c_3)^{1/3}/40$, $\frac{1}{4}$, 49, 3. The maximum and trailing-edge thicknesses and their corresponding stations are

$$\left.\begin{aligned} \tau_{1_M} &= 0.05 && \text{at} \quad x = 98^{-1/3} \approx 0.217 \\ \tau_{1_T} &= 3/2000(98)^{1/3} \approx 0.007 && \text{at} \quad x = 1, \end{aligned}\right\} \tag{6.4}$$

with τ_{2_T} being twice τ_{1_T}. The computations were performed for a Prandtl number and hypersonic interaction parameter of unity, and wall enthalpies of 0.4 and 0.2, as shown in figure 8. About 400 grid points were employed from the leading to the trailing edge, with the other conditions comparable with the case of the flat plate discussed previously. These airfoil contours start as $\tau \sim x$ rather than $x^{3/4}$ near the leading edge, i.e. less than the boundary-layer thickness, and so the similarity solution there is unaltered.

Hypersonic purely inviscid flow can also be computed using the method developed for the inviscid part of the hypersonic shock layer discussed in §3. The boundary-layer edge function $\bar{\delta}$ is replaced by a prescribed function describing the contour of the airfoil. Therefore the flow variables in (3.9) and consequently the governing equations can be expressed without the constant C_2, that is, independently of the viscous layer. However, the starting form of the airfoil should be as $\tau(x) \sim x^{3/4}$ at most, near the leading edge, to preserve the initial similarity solution. For example, airfoils with contours such as

$$\tau = c_5 x^{3/4}(1 - x^{c_6}), \quad 0 \leqslant x \leqslant 1, \tag{6.5}$$

where c_5, c_6 are constants, and the maximum thickness

$$\tau_M = 4c_5 c_6 (3/c_7)^{3/(4c_6)}/(4c_6 + 3) \quad \text{at} \quad x = [3/(4c_6 + 3)]^{1/c_6}, \tag{6.6}$$

are considered here. In particular, the flow field at moderate and strong values of the hypersonic interaction parameter, with streamwise and transverse step sizes of 0.0002, 0.002 respectively, was computed. Figure 9 presents the position of the shock wave g, for the airfoil contours τ_3, τ_4 such that

$$\tau_3 = (\tfrac{5}{3})^{3/2} x^{3/4}(1 - x^{1/2})/4, \quad \tau_4 = 7(7/3)^{3/4} x^{3/4}(1 - x)/40; \tag{6.7}$$

the constant c_6 is $\frac{1}{2}$, unity respectively and the constant c_5 is such that the scaled maximum thickness of the airfoil is 10% of the chord. The maximum thicknesses and corresponding stations are

$$\tau_{3_M} = 0.1 \quad \text{at} \quad x = (\tfrac{3}{5})^2 = 0.36, \quad \tau_{4_M} = 0.1 \quad \text{at} \quad x = \tfrac{3}{7} \approx 0.429. \tag{6.8}$$

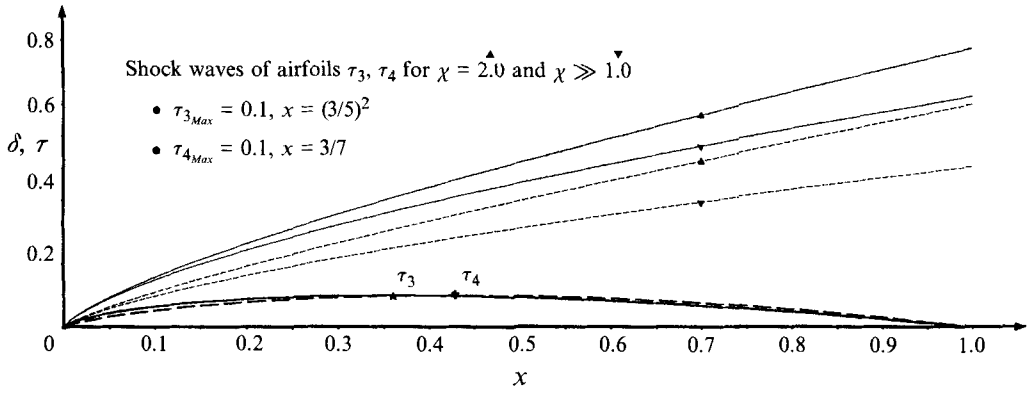

FIGURE 9. Shock wave positions g, for airfoils in inviscid hypersonic flow using forward-marching single-sweep methods (see §§6, 3).

At high values of the interaction parameter, the density at the shock wave has the constant value of 6; also the density profile changes downstream since the function $\bar{\delta}(x)$ is not constant. The computational results show that a higher number of iterations, and smaller grid size in comparison with the viscous layer, are required for the same amount of accuracy.

7. Further comments

To recap briefly first, it is observed that the viscous and inviscid layers comprising the hypersonic shock layer were computed simultaneously using finite differences and marching downstream in §3. The results showed that, as the value of wall enthalpy increases towards its insulated value (approximately $H_w > 0.1$, with insulated values of 0.4178, 0.5 for Prandtl numbers of 0.725, unity respectively), the solutions depart from the main solution downstream. Such branching occurs at different streamwise distances, depending on the values of the wall enthalpy, the hypersonic interaction parameter and the streamwise step size, owing to the upstream-influence phenomenon, as discussed theoretically in §5. However, for low values of wall enthalpy, $H_w \leqslant 0.1$ approximately, the upstream influenced is almost negligible (and probably difficult to detect experimentally) even though strictly it remains of order unity. A similar decrease in the upstream-influence length occurs at increased body thickness (see §4). Indeed, bodies with sufficiently large thickness can be analyzed using triple-deck theory centred at distances of order unity downstream along with moderate interaction. The hypersonic viscous layer can also be computed more fully by the multi-sweeping methods of §5, e.g. for high values of wall enthalpy, to accommodate the branching. The boundary-layer edge and the pressure along it are presented for a particular case in figure 10, using both the shock-layer computation with no upstream influence and the nonlinear sweep method for comparison. The methods used for the flat plate were finally modified in §6 to consider thin airfoils in hypersonic viscous flows with upstream influence and in inviscid flows.

In theoretical terms, the main point of this work is clearly that solutions for the fundamental problem of interactive hypersonic flow as posed in §2 have now been obtained, for the semi-infinite or finite flat plate and related airfoil shapes (§§3–6). As far as the authors know these are the first such solutions. The computational task, built on the flow solution's analytical properties, proved complex as expected but the

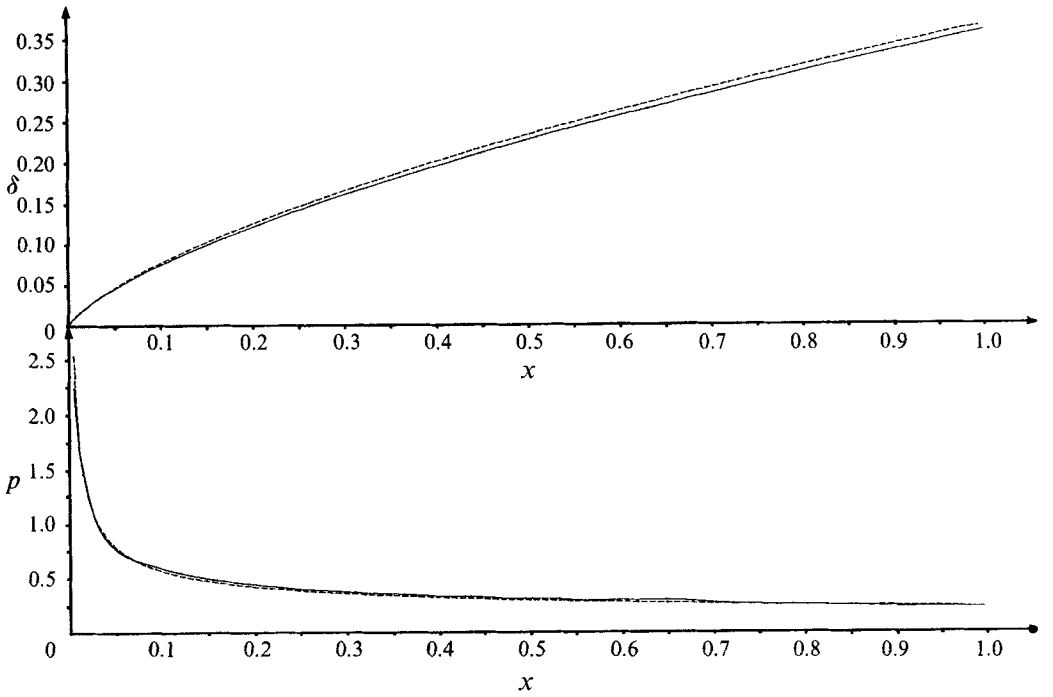

FIGURE 10. Comparison of the boundary-layer edge position δ and pressure p, using forward-marching single-sweep (——) and NLS (– – –) methods (see §§7, 3, 5). Wall enthalpy = 0.1, $Pr = 0.725$, $\chi = 1.9$.

methods developed appear to be accurate: see §§3, 5, 6 specifically and figure 4 for comparison with computational results using Navier–Stokes and parabolized Navier–Stokes equations. There are no experimental results with which direct comparisons can be made as yet, again to the best of the authors' knowledge; nevertheless the pressure and other solution curves obtained, for example in §§5, 6, are in line qualitatively with experimental measurements on various airfoil shapes.

Moreover, the results presented here are in excellent and reasonable agreement with subsequent computations of J. J. Korte (1993, personal communication), in the current parameter regime, while in other regimes his results are in good agreement with experimental data. Also, the positions of the shock waves and the wall pressure (in figures 4 and 5) are in excellent and reasonable agreements respectively with the solutions obtained with the Reduced Navier–Stokes (RNS) formulation of S. G. Rubin (1993, personal communication) and co-workers. The authors note finally here that the numerical solutions can now also be used as the basis for stability and transition calculations on the hypersonic flow over various airfoil shapes.

For practical purposes, on the other hand, probably the main benefits come from three features found during the analysis and computations. The first is rather surprising, namely that a forward-marching scheme can actually work accurately in a sense over a fairly wide range of conditions, provided that the streamwise step size, while small, is not excessively small. Compare §§3, 5 and the results in the figures. The reason is that the typical lengthscale of upstream influence is small in practice throughout, owing to the eigenvalue in §4 being large. Thus for instance the authors' results for a finite plate are found to be virtually identical with those for the semi-infinite plate, up to the onset of the trailing edge. Likewise, the influence of moving the

most downstream station in the computations of §5 is observed to be negligible in almost all of the hypersonic flow solution upstream, apart from a relatively tiny interval just prior to that station. This ability to determine many flow solutions reasonably well by means of just a single-pass computation (as in §3) is felt to be very helpful as regards practical calculations, e.g. for airfoils. Second, the wall enthalpy in reality has to be kept quite low for most flight applications and this low value reinforces the reduction in upstream-influence length described earlier in the section, see §§3–5. Similar reinforcement occurs for increasing body thickness, as shown in §4, which is again a more realistic configuration. Both of these properties therefore add further weight to the first feature described above. The third feature of practical note concerns the ability to determine hypersonic flow solutions for thicker airfoils, based on the computations in §6 and the analysis in §4. There is much interest in developing this aspect further, as it could lead to both prediction and design methods for real airfoil shapes. Related studies of nozzle flow by F.T.S. and Dr A. Neish, as reported in Brown *et al.* (1991), are pursuing similar developments.

The authors wish to express their gratitude to Professor S. N. Brown for invaluable discussions. Dr D. F. Mayers' advice on certain computational aspects was very useful. Professor S. G. Rubin is thanked for discussions on comparisons of computational results and some theoretical aspects. Dr J. J. Korte kindly provided data for comparison. Thanks are due also to Ministry of Defence (through D.R.A. Farnborough) and the Science and Engineering Research Council for their financial support and in particular to Dr T. A. Holbeche of MoD for his interest.

REFERENCES

BROWN, S. N., KHORRAMI, A. F., NEISH, A. & SMITH. F. T. 1991 On hypersonic boundary-layer interactions and transition. *Phil. Trans. R. Soc. Lond.* A **335**, 139–152.

BROWN, S. N. & STEWARTSON, K. 1975 A non-uniqueness of the hypersonic boundary layer. *Q. J. Mech. Appl. Maths* **XXVIII**, 75–90.

COWLEY, S. J. & HALL, P. 1990 On the instability of hypersonic flow past a wedge. *J. Fluid Mech.* **214**, 17–42.

HAYES, W. D. & PROBSTEIN, R. F. 1959 *Hypersonic Flow Theory*. Academic (and 2nd edn, vol I, *Inviscid Flows*, 1966).

JOBE, C. E. & BURGGRAF, O. R. 1974 The numerical solution of the asymptotic equations of trailing edge flow. *Proc. R. Soc. Lond.* A **340**, 91–111.

KHORRAMI, A. F. 1991 Hypersonic aerodynamics on flat plates and thin airfoils. D.Phil. thesis, Oxford University (Department of Engineering Science and Lady Margaret Hall).

KHORRAMI, A. F., SMITH, F. T., BROWN, S. N. & NEISH, A. 1989 Hypersonic interactions and flow transition. *Proc. R. Aero. Soc.* (*Intl Conference on Hypersonic Aerodynamics, University of Manchester*).

LEE, R. S. & CHENG, H. K. 1969 On the outer edge problem of a hypersonic boundary layer. *J. Fluid Mech.* **38**, 161–179.

LEES, L. 1953 On boundary layer equations in hypersonic flow and their approximate solution. *Readers Forum, J. Aero. Sci.* **20**, 143.

LEES, L. & PROBSTEIN, R. F. 1952 Hypersonic viscous flow over a flat plate. *Aeronautical Engineering Laboratory, Princeton University, Rep.* 195.

LIGHTHILL, M. J. 1953 On the boundary layers and upstream influence II. Supersonic flows without separation. *Proc. R. Soc. Lond.* A **217**, 478–507.

MESSITER, A. F. 1970 Boundary layer flow near the trailing edge of a flat plate. *SIAM J. Appl. Maths* **18**, 241–257.

NEILAND, V. YA. 1970 Propagation of perturbations upstream with interaction between a hypersonic

flow and a boundary layer. *Izv. Akad. Nauk SSSR, Mekh. Zhid. Gaza* **5** (4) 40–49 (English transl.).

OGUCHI, O. 1958 First order approach to a strong interaction problem in hypersonic flow over an insulated flat plate. *Aeronautical Research Institute University of Tokyo, Rep.* 330.

SHEN, S. F. 1952 On the boundary layer equations in hypersonic flow. *Readers Forum, J. Aero. Sci.* vol. 19, no. 7.

SMITH, F. T. 1983 Interacting flow theory and trailing edge separation – no stall. *J. Fluid Mech.* **131**, 219–249.

SMITH, F. T. 1989 On the first-mode instability in subsonic, supersonic or hypersonic boundary layers. *J. Fluid Mech.* **198**, 127–153.

SMITH, F. T. & BROWN, S. N. 1990 The inviscid instability of a Blasius boundary layer at large values of Mach number. *J. Fluid Mech.* **219**, 499–518.

SMITH, F. T. & KHORRAMI, A. F. 1991 The interactive breakdown in supersonic ramp-flow. *J. Fluid Mech.* **224**, 197–215.

STEWARTSON, K. 1955 On the motion of a flat plate at high speeds in a viscous compressible fluid II, steady motion. *J. Aero. Sci.* **22**, 303.

STEWARTSON, K. 1964 *The Theory of Laminar Boundary Layers in Compressible Fluids*, Oxford University Press.

STEWARTSON, K. 1968 On the flow near the trailing edge of a flat plate. *Proc. R. Soc. Lond.* A **306**, 275–290.

STEWARTSON, K. 1969 On the flow near the trailing edge of a flat plate II. *Mathematika* **16**, 106–121.

STEWARTSON, K. & WILLIAMS, P. G. 1969 Self-induced separation. *Proc. R. Soc. Lond.* A **312**, 181–206.

WERLE, M. J., DWOYER, D. L. & HANKEY, W. L. 1973 Initial profile for the hypersonic-shock/boundary-layer interaction problem. *AIAA J.* **11**, 525.